

DOI:

Characterization under Uncertainty of Catalytic Phenomena in Ceramic Matrix Composites Materials for Spacecraft Thermal Protection Systems

Diana Luís^{1,†}, Anabel del Val^{1,2,†} and Olivier Chazot¹

¹*von Karman Institute for Fluid Dynamics*

Chaussée de Waterloo 72, 1640 Rhode St-Genèse, Belgium

²*Centre de Mathématiques Appliquées, École Polytechnique*

Route de Saclay, 91128 Palaiseau Cedex, France

diana.luis@vki.ac.be · ana.isabel.del.val.benitez@vki.ac.be

[†]Corresponding authors

Abstract

This work focuses on the characterization of current spacecraft thermal protection materials, including experimental and model uncertainties. The catalysis phenomena affecting re-usable heat shield materials is considered in the physical model through a parameter that represents the exothermic recombination of atoms taking place at the material surface. Uncertainty distributions of this recombination parameter are obtained by means of a Bayesian inference framework where the model parameter is inferred from experimental data generated in a plasma wind tunnel. The testing methodology developed confirms to be a reliable experimental approach for characterizing the material and the enthalpy of the flow.

1. Introduction

Space travel, since its beginnings in Low Earth Orbit (LEO) to the exploration of our Solar System, has led to countless scientific advancements in what it is one of the most challenging undertakings of humankind.

From travelling to LEO, to the Moon landings and the exploration of Mars and distant asteroids, traveling around and beyond the orbit of our planet requires large amounts of energy, reaching velocities of the order of 7-11 km/s. All this amount of kinetic and potential energy, dictated by orbital mechanics, is dissipated when a space vehicle enters dense planetary atmospheres. The bulk of this energy is exchanged during the entry phase by converting the kinetic energy of the vehicle into thermal energy in the surrounding atmosphere through the formation of a strong bow shock ahead of the vehicle. In general, a large fraction of the energy dissipated to the atmosphere is carried away from the vehicle through convection and radiation, leaving a small percentage to be absorbed back into the vehicle as thermal energy. A Thermal Protection System (TPS) is used to mitigate this heat load and ensure that the temperature limits of critical components on board are not exceeded during the entry phase. Prediction of the heating rate which is experienced by the TPS remains an imperfect art, leading to very large safety margins for the vehicle design. Failing to correctly predict the heat loads and associated material response of the TPS during the design phase can lead to catastrophic mission failure. To address this problem, experimental facilities capable of generating high speed and plasma flows are developed to study different aspects of atmospheric entry flows,¹ together with physico-chemical models used to describe the state of the flow at a given time and conditions.² The delicate interplay between experiments and models represents the main source of knowledge about the physical phenomena and their coupling mechanisms.

Reusable heat shields are used for moderate entry velocity vehicles to dissipate heat by re-radiating the energy back into the flow, and are designed to withstand multiple uses without need for replacement or repair.³ They are typically constructed from carbon or silicon carbide materials which have high emissivities at high temperatures to promote re-radiation. The interaction between the dissociated gas and the protection system is governed by the material behavior which acts as a catalyst for exothermic recombination reactions of the atomic species in the surrounding gas mixture.⁴ The determination of the catalytic properties of thermal protection materials is a difficult task subjected to experimental and model uncertainties, and the design and performance of reusable atmospheric entry vehicles must account for these uncertain characterizations.

CHARACTERIZATION UNDER UNCERTAINTY OF CMC MATERIALS

The catalytic behavior of these materials cannot be assessed just experimentally. The experiments are coupled with numerical simulations to rebuild from the measurements the free stream enthalpy and the recombination parameters.⁵ The logic of the rebuilding consists on measuring certain quantities of interest under relevant testing conditions in the VKI Plasmatron, namely wall heat fluxes, temperatures and pressures, and use them as input conditions for a numerical solver that reproduces the boundary layer in front of the probe. The information needed to reproduce this chemically reacting boundary layer comes from the outer layer conditions and the wall conditions, namely, the material catalytic properties and surface temperature. In the absence of knowledge about the outer edge conditions or the material conditions, whichever can be rebuilt from the information of the other through iterative methods for the computed boundary layer when targetting to fit the available measurements. In this work, the outer edge conditions are represented by the enthalpy of the flow at the boundary layer edge while the wall conditions are defined by a catalytic parameter for each material.

Traditionally, the experimental testing of such catalytic thermal protection materials is carried out using two different probes holding two different materials: a designated reference (or auxiliary) material and the TPS material in question. Both materials are tested under the same flow conditions at a time. The rebuilding of such properties is heavily based on the choice of the auxiliary material, whose catalytic properties are considered well-known. The reasoning behind this is that the catalytic behavior of the TPS material can be determined by performing a two-step rebuilding. The wall conditions for the reference material are well-known so the outer edge conditions are rebuilt. As both materials are tested under the same outer edge conditions (during the same run of the plasma wind tunnel), the wall conditions for the material under study can be rebuilt from the knowledge of the outer edge conditions. This experimental approach comprises the state-of-the-art for catalytic thermal protection systems characterization at VKI.⁵ Viladegut⁶ took this exercise further by characterizing the catalytic properties of the most common reference material used in the experiments, copper. Through his work, Viladegut developed a 3-probes testing methodology aimed at characterizing well copper catalytic properties for future uses on experiments with TPS materials.

Building on the works of Panerai⁵ and Viladegut, this contribution designs a new experimental setup, aimed at characterizing TPS materials very accurately without making any assumptions on the flow outer edge properties or the reference materials catalytic properties. This new experimental setup combines the advantages of the 3-probes methodology developed by Viladegut with the testing of actual TPS materials and not just reference probes as done by Panerai.

As shown by Sanson et al.,⁷ a fully Bayesian approach combining all set of available measurements can be used to infer the catalytic properties of different materials, while treating them as equal in the priori knowledge. For this work, the new experimental setup is used to get the measurements and a more accurate Bayesian inference framework is used to infer the catalytic parameters for a full characterization including uncertainties in the measurements and in the knowledge of the reference probes. This way of treating and learning model parameters from the data proves to be very reliable from the fact that gets rid of problematic assumptions and leads the way of improving future characterizations by designing informative experiments in the most relevant conditions as shown in this work. Overall this effort represents a cornerstone in the study and analysis of this parameter from an experimental and mathematical perspective.

2. Experimental facility, measurement techniques and methods

The experimental setup installed at the Plasmatron facility offers intrusive and non-intrusive (optical) measurement techniques. The instrumentation equipment for this work consisted of a 2-color pyrometer, a broad-band radiometer and probes for heat flux and pressure measurements. The main data of interest during this investigation were heat fluxes for the three different materials and surface temperature for the TPS material.

2.1 Plasmatron facility description

The Plasmatron at von Karman Institute (VKI) is an inductively-coupled plasma (ICP) wind tunnel,⁸ that offers an ideal environment for catalytic studies due to the production of plasma jets of very high chemical purity.⁵ This facility has been extensively studied by Bottin⁹ and Bottin et al.⁸ and a detailed description may be found in their works. Its basic concept consists of a quartz tube surrounded by a coil, which is connected to a generator that provides high voltage (1.2 MW) and high frequency (400 kHz) current. This induces an electromagnetic (EM) field inside the tube, that forces residual charged particles in the flow to form eddy currents which heats up the gas by Joule effect. The injection of gas is done through a ring-shaped inlet at the outer edge of the torch. Due to the induced EM field, the gas ionizes into plasma flow, which exits at subsonic speed into a low pressure test chamber that hosts material probes. Argon is employed as starting gas, facilitating the initial electric discharge, due to the longer lifetime of the free electrons at low pressure compared to the air plasma case. Complementary systems are responsible for the gas

circulation, probes, cooling, and diagnostics. TPS material and two reference probes (copper and quartz) are mounted onto holders which are remotely activated to be injected and retracted from the plasma jet. Suitable windows provide the necessary optical access to the testing chamber for the flow and sample diagnostics: the lateral windows (on both sides of the wind tunnel) allow perpendicular side views of the plasma jet and probes, and the the torch-side windows allow a frontal oblique view of the TPS surface.

2.2 Experimental setup and methods

To characterize a TPS material in a ground facility, the environment under which the probe is hosted needs to be known. To calibrate the plasma flow conditions, two water-cooled probes are used. Two 14 mm (sensing area) copper and quartz calorimeters measure the cold wall ($\approx 350\text{K}$ and $\approx 750\text{K}$, respectively) heat flux at the stagnation point. These heat fluxes are determined by the water mass flow (\dot{m}), which is controlled by a calibrated rotameter, and the temperature difference ($T_{\text{out}} - T_{\text{in}}$) in the cooling water supply. Thus, the heat flux for the cold wall (q_{cw}) probes is given by

$$q_{\text{cw}} = \frac{\dot{m}c_p(T_{\text{out}} - T_{\text{in}})}{A} \quad (1)$$

where c_p is the water specific heat and A the area of the surface of the probe. The heat flux probe is injected into the plasma flow once the air mass flow and chamber pressure are stabilized. The total pressure (P_T) is measured using a Valydine differential pressure transducer and the static pressure (P_s) in the Plasmatron chamber is measured by an absolute pressure transducer (Memberanovac DM 12, Leybold Vacuum, OC Oerlikon Corporation AG). Then, based on this measurements, the dynamic pressure ($P_{\text{dyn}} = P_T - P_s$) is recorded. As the Plasmatron only has three probe holders, the dynamic pressure is recorded during a different test case, where the copper heat flux and pressures of the first experimental run are duplicated.

Figure 1 presents the experimental setup adopted for this study. Copper, TPS and quartz samples are mounted on probe holders. In this work, "standard" ESA geometry probes (also known as Euromodel) for typical non-equilibrium boundary layers, with a radius of 25 mm, are used. To analyse the surface temperature and emissivity of the TPS material, a two-colour pyrometer and an infrared radiometer are used. As previously mentioned, heat flux and pressure probes are used for jet calibration.

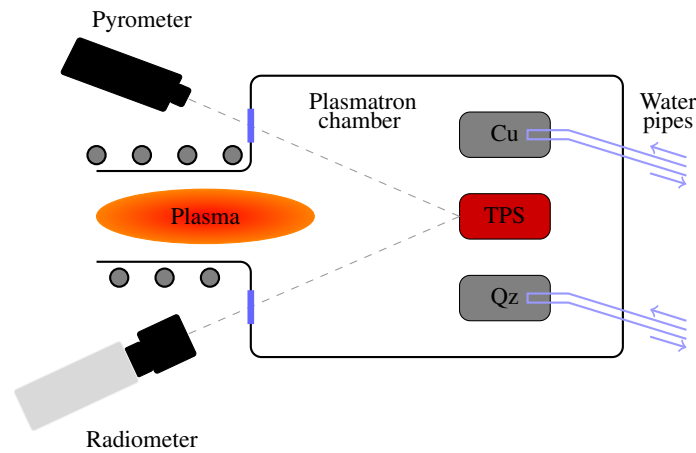


Figure 1: Schematic of experimental setup (seen from top, not to scale) with pyrometer and radiometer optical path in front of the TPS material sample.

The optical instruments as the pyrometer and radiometer are calibrated with the aid of a black-body (BB) source (LANDCAL R1500T, LAND Instruments International), which provides a reference temperature spot with an emissivity value close to 1. The calibration curves presented in this report were provided by Helber.¹⁰ A two-colour Raytek Marathon Series MR1S-C infrared pyrometer with an operating range between 1000°C and 3000°C is used. Optical access to the testing chamber is offered through a 1 cm thick quartz window, placed at ~ 1 m distance to the probe, with an orientation of $\sim 35^\circ$ with respect to the stagnation line.

To record the surface radiance, a broadband infrared radiometer (KT19, HEITRON-ICS Infrarot Messtechnik GmbH) is used. This instrument is located at $\sim 47^\circ$ angle relative to the surface normal in front of a 1.8 cm thick KRS-5 window, which offers $\sim 70\%$ optical transparency⁵ in the whole infrared range of the instrument ($0.6 - 0.39\mu\text{m}$). Its

CHARACTERIZATION UNDER UNCERTAINTY OF CMC MATERIALS

temperature range is between 0°C and 3000°C and the acquisition frequency is set to 1 Hz. The output provided is the integrated thermal radiation over the spectral range, converted into equivalent temperature through an adjustable emissivity value which, in the context of the Plasmatron facility, is set to one.

As the range between 0.6 – 0.39 μm contains the highest percentage of thermal radiation at the operation temperatures of the Plasmatron,⁵ the actual radiance and emissivity can be computed with the Stefan-Boltzmann law. Being T_w^{pyro} the real surface temperature acquired by the pyrometer and T_w^{radio} the equivalent temperature measured by the radiometer, the total emissivity can be determined as

$$\varepsilon = \frac{(T_w^{\text{radio}})^4}{(T_w^{\text{pyro}})^4}. \quad (2)$$

Among the experimental testing, there are uncertainties associated to the measured flow parameters as the static pressure, P_s , dynamic pressure, P_{dyn} , and cold wall heat fluxes, $q_{\text{cw}}^{\text{Cu}}$ and $q_{\text{cw}}^{\text{Qz}}$; to the measured surface parameters as the surface temperature, T_w^{TPS} , and emissivity, ε ; and to the cold wall temperatures assumptions, $T_{\text{cw}}^{\text{Cu}}$ and $T_{\text{cw}}^{\text{Qz}}$. For Uncertainty Quantification (UQ), these are the uncertainties that are treated as aleatory variables with Gaussian distributions.

2.3 On the differential pressure transducer measurements

As previously mentioned, the experiments are performed with three sample probes (copper, TPS and quartz). Therefore, there is no place available for the pressure transducer and, consequently, the measurement of the dynamic pressure cannot be obtained simultaneously. Hence, a second experimental run is performed with the water-cooled copper probe, to perform again the calibration of the plasma flow and to try to duplicate the testing conditions obtained in the first experimental run. Simultaneously, a pressure transducer is mounted on another holder.

As the copper heat fluxes cannot be exactly duplicated in both experimental runs, a correction factor must be applied to obtain the real dynamic pressure. As the dynamic pressure is linearly proportional to the heat flux,⁶ for static pressures of 15 and 100 mbar, linear regressions are obtained with the values measured in the second experimental run. Once the copper heat fluxes are obtained in the first experimental run, the real values of the dynamic pressure are computed. For a static pressure of 50 mbar, as there is just one point measured, the dynamic pressure is corrected multiplying the measured pressure by the ratio between the heat fluxes of the first and the second experimental runs.

3. Numerical Solvers and Uncertainty Quantification Methodology

The characterization of reusable thermal protection materials by estimation of the catalytic parameter requires performing tests in a relevant and similar environment. These experiments are then coupled with numerical simulations to rebuild from the measurements the enthalpy and recombination parameters. As experiments and models have associated uncertainties, these must be integrated into the numerical framework as well.

3.1 Numerical solvers for catalysis and enthalpy rebuilding

The logic of the rebuilding consists on measuring certain quantities of interest under certain testing conditions in the Plasmatron, and using them as input conditions for two numerical solvers that reproduce the flow around the probe. The rebuilding method provides a simulation of the chemically reacting boundary layer at the stagnation line, together with all the thermodynamic properties, from the outer edge to the wall.

The first software is an in-house Inductively-Coupled Plasma (ICP) solver available within the CoolFluid¹¹ platform. This solver helps to define the framework of the problem to be solved around the probe by simulating the interaction between the electromagnetic field around the coil and the gas passing through, with the aim of reproducing the whole Plasmatron chamber. ICP simulations are in Local Thermodynamic Equilibrium (LTE) conditions, which is reasonable away from both the torch exit and the probe.¹² The purpose of the LTE viscous flow computation is to compute the values of non-dimensional parameters (NDPs), Π_i , which characterize the flow near the stagnation point of the heat flux probe in the plasma jet for a selected mass flow rate.¹³

The operating conditions of the Plasmatron are defined by the gas mass flow, \dot{m} , static pressure, P_s , and power, P_w . These quantities together with the probe configuration (or the probe radius r_p) are used as input for the ICP simulations. Their outputs are then used as inputs for CERBOULA in the form of the NDPs obtained from the LTE viscous flow simulation.¹³ In the context of this work, however, the ICP code is not used and the correlation provided by Panerai⁵ is implemented for this purpose.

The second software intervening in the rebuilding process is the so-called CERBOULA, a coupling between the NEBOULA (Non-Equilibrium BOUNDary LAYer) solver and the CERBERE (Catalycity and Enthalpy ReBuilding on a REFerence probe) routine. The first was developed by Barbante¹⁴ at VKI and assumes thermal equilibrium and chemical nonequilibrium to compute both the gas thermodynamic and transport properties along the stagnation line in different flow configurations. The condition of LTE is imposed at the boundary layer edge while the surface temperature and the catalytic parameter are introduced as wall boundary conditions. NEBOULA is then plugged into CERBERE routine to be used as a tool for Plasmatron data rebuilding. The input variables of the ensemble CERBOULA are a combination of measured quantities in the Plasmatron and some hydrodynamic outputs from the ICP simulation. CERBOULA ultimately computes the boundary layer edge conditions in front of the probe.

To compute a relationship between the boundary layer edge enthalpy and the catalytic parameter, the static and dynamic pressures, wall temperatures and heat fluxes measurements together with the NDPs are used as variables for the Boundary Layer code. In this scenario, the heat flux can be expressed as function of the input parameters

$$q_w = q_w(H_e, T_w, P_s, \Pi_i, \dots, \gamma_i) \quad (3)$$

and either the enthalpy nor the catalytic parameter have to be assumed to have a complete rebuilding characterization. As the heat flux is a measured quantity, the solver iterates until the numerical heat flux coincides with the experimental heat flux, as illustrated in Fig. 2.

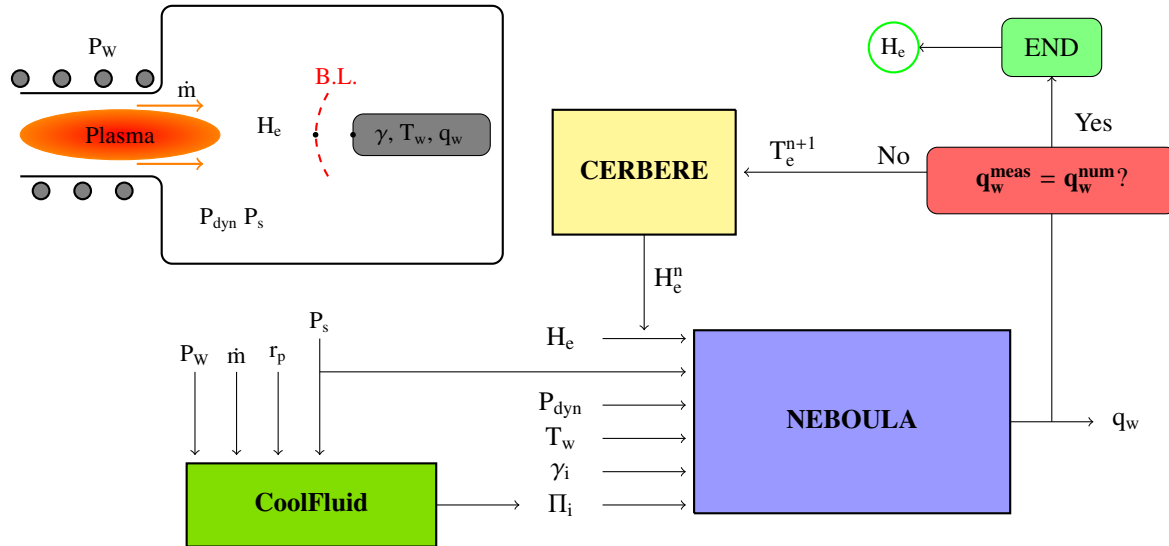


Figure 2: Conventional enthalpy rebuilding workflow for the plasma jet characterization in the Plasmatron. The same workflow applies to the case when we want to estimate γ_i instead of H_e , being the latter known or assumed.

3.2 Uncertainty Quantification methodology

The determination of catalytic properties is affected by the noise present in the experimental data, even for well-characterized facilities, together with theoretical assumptions that must be also evaluated. Hence, the uncertainties associated with the experiments and rebuilding methodology must be integrated into the numerical framework, to obtain a more reliable prediction of the catalytic parameter.

In most of the experimental approaches, the authors rely on the knowledge of the reference calorimeter catalytic property which is not an adequate assumption.¹⁵ Therefore, the catalytic property for copper and quartz should also be included as unknowns in the rebuilding process. In this Bayesian inference approach, references and TPS material catalytic properties play the same role in the inference process, being all inferred at the same time.

3.2.1 Prior distribution and likelihood function

According to the Bayes rule, the posterior distribution of any quantity of interest can be divided into a ratio of probabilities. In the case of this work, this ratio reads

$$P(\gamma_{Qz}, \gamma_{TPS}, \gamma_{Cu} | M) = \frac{L(M | \gamma_{Qz}, \gamma_{TPS}, \gamma_{Cu}) P(\gamma_{Qz}, \gamma_{TPS}, \gamma_{Cu})}{P(M)}, \quad (4)$$

CHARACTERIZATION UNDER UNCERTAINTY OF CMC MATERIALS

where $M = (q_{cw}^{Qz}, q_{cw}^{Cu}, T_{cw}^{Qz}, T_{cw}^{Cu}, q_w^{TPS}, T_w^{TPS}, P_s, P_{dyn})$ is the set of available measurements and $\gamma_{Qz}, \gamma_{TPS}, \gamma_{Cu}$ are the recombination parameters to be inferred; $L(M|\gamma_{Qz}, \gamma_{TPS}, \gamma_{Cu})$ refers to the likelihood of the data measured M , given the model parameters $\gamma_{Qz}, \gamma_{TPS}$ and γ_{Cu} ; $P(\gamma_{Qz}, \gamma_{TPS}, \gamma_{Cu})$ is the prior probability distributions of the model parameters and $P(M)$ is the marginal likelihood, that is, the probability that the considered measurements are obtained. All prior probability distributions are taken as log-uniform in within selected intervals, with constraints on the normalization factor (integral of the distribution is equal to one). In this way, no assumptions are made about the catalytic behavior of the reference probes compared to the one of the material under study. This choice of priors also ensures compliance with the maximum entropy principle.¹⁶

As both materials should play the same role in the inference problem, a likelihood function accounting for the whole set of available measurements was designed, including reference probes and TPS material catalytic properties. This likelihood function quantifies the amount of information carried by the measurements to the Quantities of Interest (QoI) and it measures the compatibility between the measurements and the value of unknown model parameters, such as the recombination parameters. Nevertheless, this likelihood function has two problems. First, the model predictions of q_{wi} do not solely depend on $\gamma_{Qz}, \gamma_{TPS}$ and γ_{Cu} but also on the boundary layer edge enthalpy, H_e . Second, H_e is not predicted by the model, i.e., is not one of its outputs, but instead is an input of the model (as represented in Fig. 2). To tackle these issues, the model inputs that maximize the likelihood function were determined. Assuming that the available measurements are independent unbiased Gaussian, the likelihood function developed takes the form

$$L^{opt}(M|\gamma_{Qz}, \gamma_{TPS}, \gamma_{Cu}) \propto \exp\left[-\frac{|P_s^{meas} - P_s^{opt}|^2}{2\sigma_{P_s}^2}\right] \exp\left[-\frac{|P_{dyn}^{meas} - P_{dyn}^{opt}|^2}{2\sigma_{P_{dyn}}^2}\right] \prod_{i \in Qz, TPS, Cu} \exp\left[-\frac{|q_{wi}^{meas} - q_{wi}^{opt}|^2}{2\sigma_{q_w}^2} - \frac{|T_{wi}^{meas} - T_{wi}^{opt}|^2}{2\sigma_{T_w}^2}\right] \quad (5)$$

where $H_e^{opt}, P_s^{opt}, P_{dyn}^{opt}, T_{wi}^{opt}$ are the quantities that maximize the likelihood function and q_{wi}^{opt} the corresponding predictions of the heat fluxes for the three material samples. These optimal quantities are only function of the three material properties $\gamma_{Qz}, \gamma_{TPS}$ and γ_{Cu} .

The optimization process for this task is the Nelder-Mead algorithm.¹⁷ However, applying an optimization method prevents from using directly this approach to sample the posterior distribution due to high computational time. Each point of the sampling space is the result of an optimization procedure which takes in of the order of hundred realizations of the numerical solver. To overcome this limitation, a surrogate model for the log-likelihood of the problem was built.

3.2.2 Surrogate modeling and sampling of the posterior distribution

The surrogate model is built by considering the log-likelihood as a function of the log-variables, $\log_{10}\gamma_{Qz}$, $\log_{10}\gamma_{TPS}$ and $\log_{10}\gamma_{Cu}$, using Gaussian Processes (GP). It is considered this way due to smoothness of the approximated function (log-likelihood as function of the log-variables) while sharing the behavior and optimal values as the original likelihood function. Due to their statistical nature, GP provide both a prediction of the approximated function and a measure of the uncertainty (variance) in the prediction. To this end, three dimensional grid in the plane of the log-variables is considered and the corresponding values of the log-likelihood evaluated. In this case, the choice of sampling the QoIs space is by using Latin Hypercube Sampling (LHS) techniques,¹⁸ together with a sequential approach to the posterior sampling. This approach starts with a LHS sparse grid upon which the first GP surrogate is built.¹⁹ The GP surrogate is used in place of the exact likelihood function to sample the posterior distribution by means of the Metropolis-Hastings algorithm,²⁰ a flavour of Markov Chain Monte Carlo (MCMC).²⁰ In subsequent iterations of this procedure, the additional sampling domain can become smaller, focusing only on the part of the 3D domain where MCMC is drawing samples from, refining the accuracy of the GP in that part. The stopping criteria is chosen when the standard deviation of the GP, used as a measurement of its error, is less than 1% the mean value. It was concluded that GP yield good results with low standard deviations on the chain samples. Moreover, the approach is robust, meaning that the MCMC sampling method works smoothly for any given conditions.

4. Results and discussion

In this section, the methodology previously discussed is applied for experimental cases performed at the VKI Plasmatron. All these cases are analyzed under the Bayesian framework to characterize the catalysis behavior of the CMC material with the experimental results obtained in this work.

4.1 Test conditions

To proceed with the experiments, the Plasmatron is switched on and the air mass flow is set with a calibrated rotameter. The vacuum pumps are then regulated until the target static pressure is reached inside the chamber. After that, the probe with the copper calorimeter is injected into the plasma and power is regulated according to the target heat flux being measured, displayed and recorded in real-time. Once the calorimeter reaches a steady-state signal under the imposed conditions, the probe is removed from the plasma jet and that holding the quartz calorimeter is introduced. The heat flux is measured and the injection/ejection process is repeated for the TPS sample. Tables 1 and 2 summarize the experimental testing conditions and associated uncertainties based on the tests carried out with the setup depicted in Sec. 2.2.

Table 1: Plasmatron test conditions (15, 50 and 100 hPa, atmospheric air): targetted cold wall heat flux $q_{cw}^{Cu,ref}$, dynamic pressure P_{dyn} , mean cold wall heat fluxes q_{cw}^i , mean surface temperature T_w^{TPS}

Test case	P_s (mbar)	$q_{cw}^{Cu,ref}$ (kW/m ²)	P_{dyn} (Pa)	q_{cw}^{Cu} (kW/m ²)	q_{cw}^{Qz} (kW/m ²)	q_w^{TPS} (kW/m ²)	T_w^{TPS} (K)
MTAt1	15	500	121.48	493.57	219.35	227.79	1462.9
MTAt2	15	700	160.31	702.76	317.90	346.48	1631.0
MTAt3	15	900	196.6	898.39	374.13	417.23	1698.4
MTAt4	50	700	37.40	694.22	258.18	324.75	1585.6
MTAt5	100	500	13.60	492.56	251.00	302.49	1566.5
MTAt6	100	700	16.60	691.56	277.38	381.94	2655.8
MTAt7	100	900	19.62	892.48	337.04	470.45	1741.4

These experimental test cases are chosen to study the impact of changing the heat flux for the same pressure. Hence, heat fluxes of 500, 700 and 900 kW/m² are tested. Additionally, a higher static pressure (100 mbar) is tested for the same heat fluxes. Thereafter, the impact of changing heat fluxes and pressures can be compared in the posterior analysis. These cases are representative of material behaviors of copper, quartz and TPS yielding good posterior distributions for the TPS material. Therefore, they are chosen along with additional conditions for a comprehensive study of the catalysis phenomena.

Table 2: Experimental conditions uncertainties

Test case	P_s (mbar)	δP_s (mbar)	δP_{dyn} (Pa)	δq_{cw}^{Cu} (kW/m ²)	δq_{cw}^{Qz} (kW/m ²)	δq_w^{TPS} (kW/m ²)	δT_w^{TPS} (K)
MTAt1	15	0.15	2.31	43.87	19.43	21.37	21.94
MTAt2	15	0.15	2.52	62.60	28.43	32.55	24.46
MTAt3	15	0.15	2.39	79.76	33.29	39.14	25.47
MTAt4	50	0.50	2.64	61.19	22.86	30.50	23.78
MTAt5	100	1.00	2.50	43.54	22.20	28.37	23.49
MTAt6	100	1.00	2.54	61.02	24.58	35.83	24.83
MTAt7	100	1.00	2.58	79.10	29.90	44.13	26.12

In the tests performed for this work, the static pressure was not recorded. Hence, a $\pm 10\%$ uncertainty is considered, due to the stability of the pump regulating the vacuum conditions. This assumption was previously applied by different authors working on the Plasmatron as Panerai,⁵ Viladegut⁶ and Fagnani.²¹ Uncertainties estimates for the wall temperature are also taken from Helber.²²

For the cold wall heat fluxes, there are experimental uncertainties associated with the measurement chain (MC) used in the Plasmatron. According to Bottin,⁸ for the cold wall heat flux, the uncertainty estimate due to this chain is given by

$$\delta q_{(i)}^{MC} = \frac{0.089}{2} q_{(i)}^{(i)}, \quad (6)$$

where (i) are both copper and quartz and $q_{(i)}^{(i)}$ the corresponding final heat flux. However, these measurements are performed for a given time with a given frequency and then averaged over the selected points that are considered as relevant. Due to this procedure, there is an associated uncertainty associated to the fluctuations of measurements over

CHARACTERIZATION UNDER UNCERTAINTY OF CMC MATERIALS

time. These type of uncertainties are computed as

$$\delta q_{(i)}^{fluct} = \frac{\sigma_{q_{(i)}}}{\sqrt{N}}, \quad (7)$$

where $\sigma_{q_{(i)}}$ is the standard deviation of the finite number of selected points to average the heat flux and N the number of those selected points. As the number of points is not infinite, a normal distribution cannot be assumed. Thereafter, a t-Student distribution should be taken into consideration when computing the confidence interval. The final uncertainty for the heat flux is computed as

$$\delta q_{total} = \sqrt{(q_{(i)}^{MC})^2 + (q_{(i)}^{fluct})^2} \times t_{factor}, \quad (8)$$

where t_{factor} is the t-Student factor considering a 95% confidence interval for the number of degrees of freedom of the measurement ($N-1$).

The same procedure is followed for the dynamic pressure yielding the results depicted in Table 2. Hot wall measurement uncertainties are computed as a results of applying Taylor expansions to the radiative equilibrium condition $q_w^{TPS} = \sigma_B \varepsilon (T_w^{TPS})^4$, where the uncertainties associated with the emissivity are computed through Taylor expansions applied to Eq. 2.

4.2 Experimental and numerical results

From all the experimental conditions, three of them, MTAt1, MTAt2 and MTAt4, are chosen to be highlight. These three conditions present different tendencies and quality of the results that make them worth exploring in more detail. The analysis of the other cases tested in the context of this work fit well within any of these three tendencies.

4.2.1 MTAt1 results and analysis

Starting with MTAt1, Fig. 3 illustrates the S-curves for this experimental condition. As previously explained, for a 3-probes methodology, the possible enthalpy range varies between the maximum enthalpy for quartz and the minimum enthalpy for copper. In this case, this range is narrow, defining, consequently, a narrow range of the TPS catalytic parameter.

The samples that maximize the likelihood function and, consequently, used for the construction of the posterior distributions are represented in Fig. 4, together with the S-curves and respective 2σ uncertainties limits. As the majority of the samples belong inside these limits, the inference is successful.

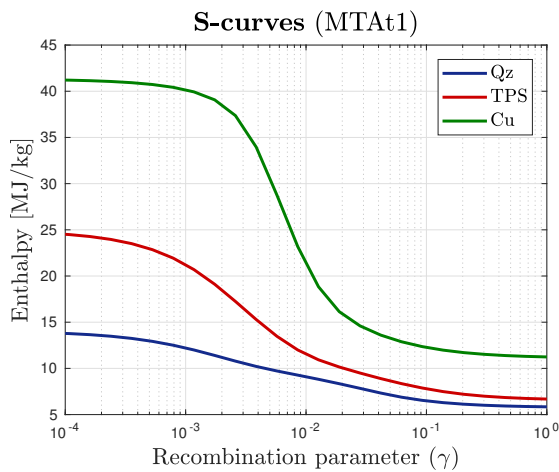


Figure 3: S-curves computed by the boundary layer solver as a relationship between the two unknowns of the rebuilding: H_e and γ

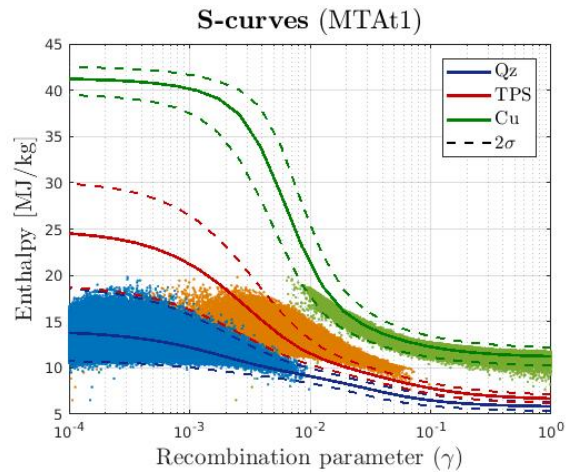


Figure 4: S-curves variability due to measurement uncertainties

The TPS posterior distribution (Fig. 5) presents a peak at around 0.015, with a wide range of possible values, varying between 0.001 and 0.06. Simultaneously, the other two parameters present a flat distribution for low catalysis and high catalysis, respectively, for quartz and copper. This flatness is due to the part of the S-curves where the computed samples lay on. Catalysis values higher than 0.007 are excluded for quartz and values lower than 0.01 excluded for copper.

The enthalpy distribution (Fig. 6) also presents a very wide range of possible values as the information of the free stream is not captured well enough.

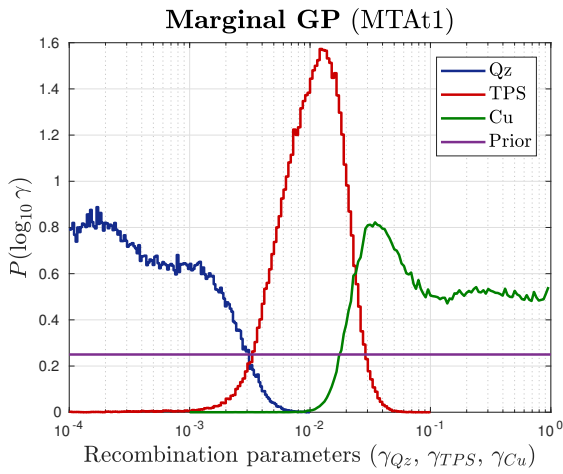


Figure 5: Marginal posterior distributions for the recombination parameters of the three probe materials

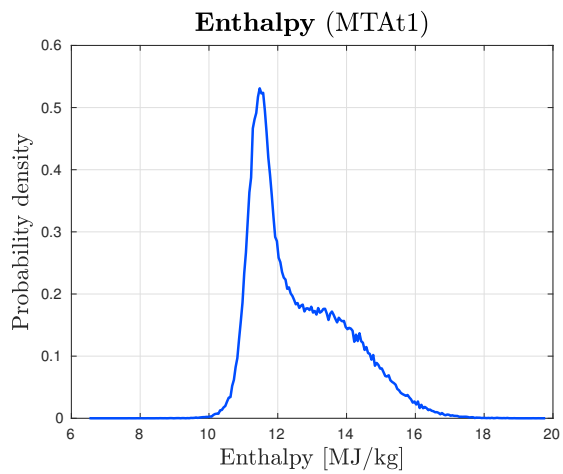


Figure 6: Resulting enthalpy distribution for the free stream flow

4.2.2 MTAt2 results and analysis

Following the detailed analysis, the S-curves presented in Fig. 7 are very closed together, yielding a very similar behavior of copper and quartz and, consequently, a very wide range of values for the enthalpy. For this case, 95% of the MCMC samples computed fit inside the 2σ uncertainty limits (Fig. 8).

Due to the wide range of possible values for the enthalpy, the values that maximize the likelihood function are spread around the sampling space and, consequently, the TPS marginal distribution presents a bimodal distribution with two peaks (Fig. 9), as well as the enthalpy distribution (Fig. 10). From the shape of these distributions, the points with higher probability of occurring fall into two different groups, decreasing the probability density among them. For this case, the TPS material admits recombination parameters between 0.001 and 0.05, with two peaks at 0.007 and 0.02, the latest having higher probability. Due to the increased overlapping, the points of the reference materials are shifted towards the steep part of the S-curves, translating into a more peaky behavior in the posteriors. The peaks are found at $\gamma_{Cu} \approx 0.015$ and $\gamma_{Qz} \approx 0.005$. Catalysis parameters lower than 0.006 and higher than 0.02 are excluded, respectively, for copper and quartz.

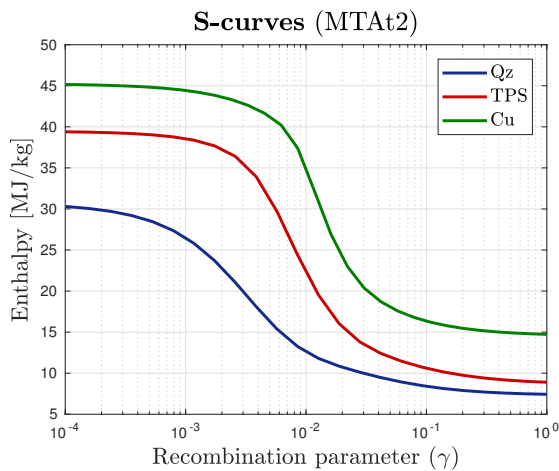


Figure 7: S-curves computed by the boundary layer solver as a relationship between the two unknowns of the rebuilding: H_e and γ

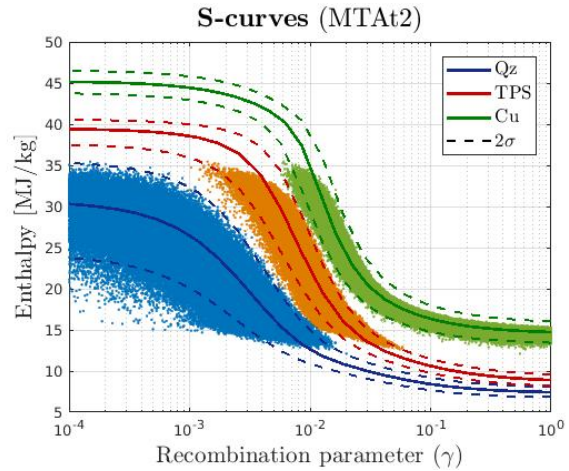


Figure 8: S-curves variability due to measurement uncertainties

CHARACTERIZATION UNDER UNCERTAINTY OF CMC MATERIALS

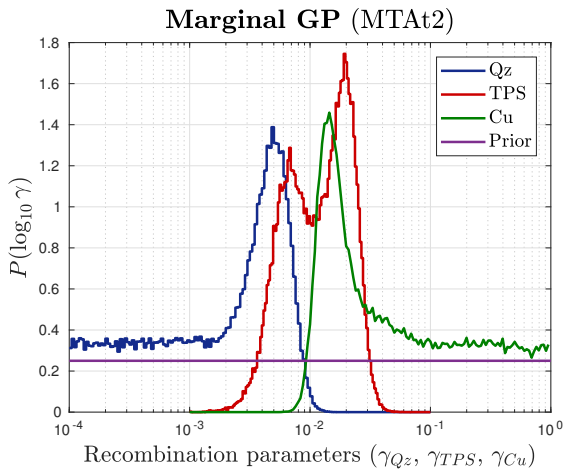


Figure 9: Marginal posterior distributions for the recombination parameters of the three probe materials

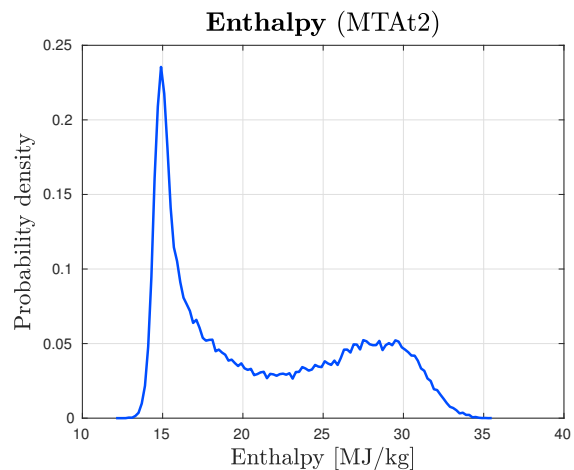


Figure 10: Resulting enthalpy distribution for the free stream flow

The results concerning the test case of MTAt3 are qualitatively similar to the case of MTAt2. Marginal posterior distributions are yielded for the three catalytic parameters as seen in Fig. 11, with a similar spread in the enthalpy distribution (Fig. 12). This is due to the overlap of the S-curves in the enthalpy sense. MTAt2 and MTAt3 share the order of magnitude of this overlap, yielding the same qualitative inference results.

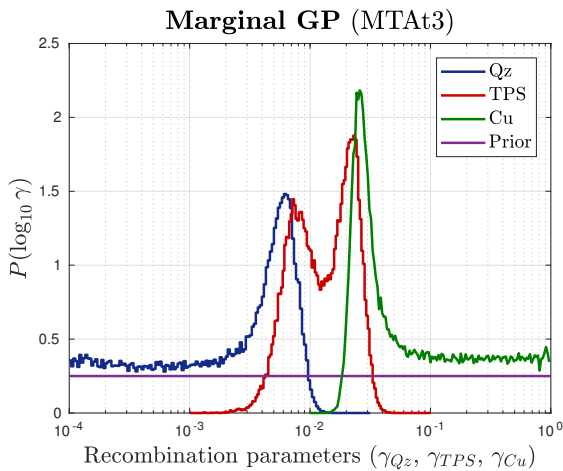


Figure 11: Marginal posterior distributions for the recombination parameters of the three probe materials

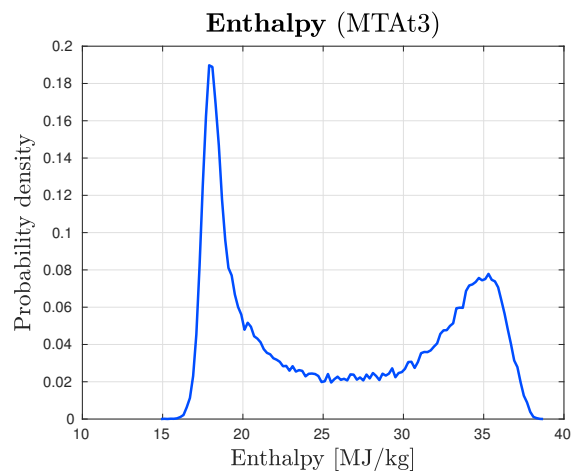


Figure 12: Resulting enthalpy distribution for the free stream flow

4.2.3 MTAt4 results and analysis

Figure 13 presents the S-curves for the fourth experimental case and, apparently there is no solution for the enthalpy. The uncertainties associated with the measurements can account for these discrepancies.

To analyse the viability of the results, the samples that maximize the likelihood function and that are used for the construction of the posterior distribution are plotted together with the S-curves and the 3σ uncertainty limits (Fig. 14). For this 99% confidence interval, less than 1% of the points are outside of the limits and, hence, the inference is successful and the uncertainty measurements can account for these discrepancies.

From the chain samples (Fig. 14) and the posterior distribution (Fig. 15), the range of values for γ_{TPS} varies between 0.002 and 0.01, with a very well-defined peak at $\gamma_{TPS} = 0.005$.

For the reference materials, the possible values for γ are also contained in a narrow region, being values higher than 0.001 and lower than 0.02 excluded, respectively, for quartz and copper. As the samples for these materials lay in the flat part of the respective S-curve, the most peaky part of the posterior distribution occurs at the lowest and highest extremes, respectively, for quartz and copper.

As the posterior distribution for the TPS is very well-defined, the enthalpy distribution (Fig. 16) resembles a Gaussian distribution with possible values varying between a narrow range.

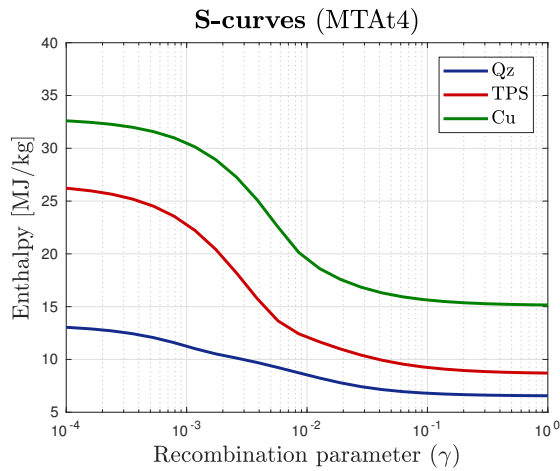


Figure 13: S-curves computed by the boundary layer solver as a relationship between the two unknowns of the rebuilding: H_e and γ

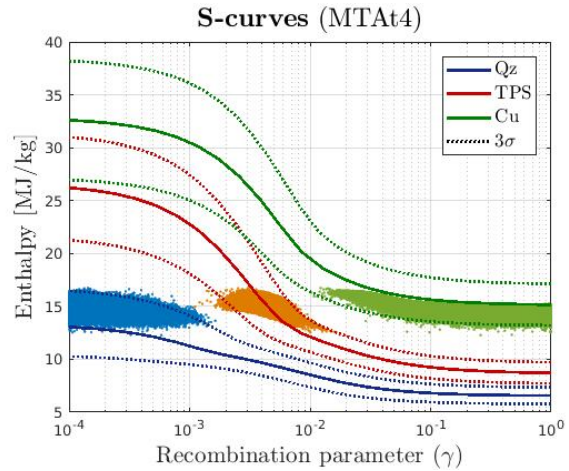


Figure 14: S-curves variability due to measurement uncertainties

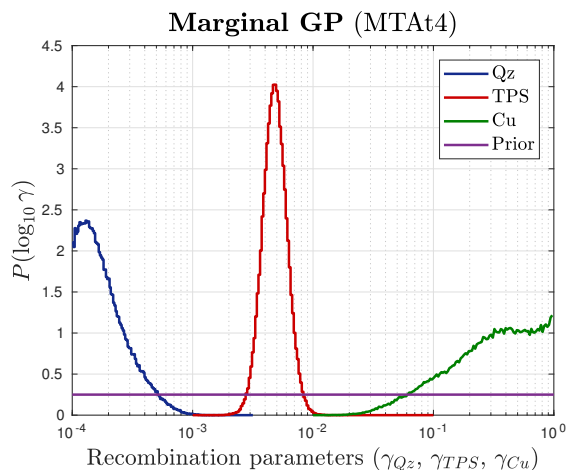


Figure 15: Marginal posterior distributions for the recombination parameters of the three probe materials

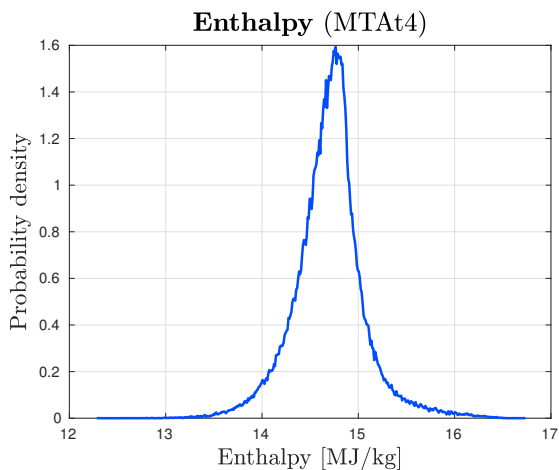


Figure 16: Resulting enthalpy distribution for the free stream flow

The results concerning the test case of MTAt5 are qualitatively similar to the ones from case MTAt4. The marginal posterior distributions for the three catalytic parameters are represented in Fig. 17 with a similar spread in the enthalpy distribution (Fig. 18) as in case MTAt4.

Taking this overlap a little further apart is where MTAt6 and MTAt7 lay. For these two cases the inference is not reliable and results are not physical as the points fall out of the limits for the measurement uncertainties. For this reasons these test cases are not analysed here.

CHARACTERIZATION UNDER UNCERTAINTY OF CMC MATERIALS

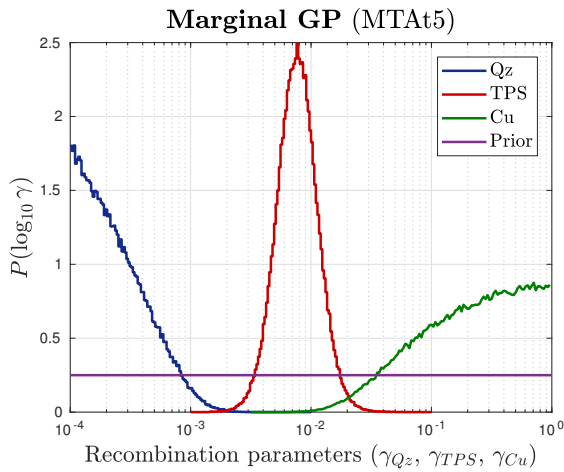


Figure 17: Marginal posterior distributions for the recombination parameters of the three probe materials

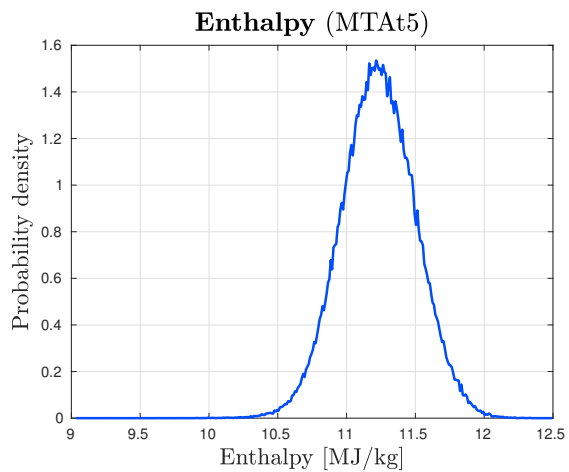


Figure 18: Resulting enthalpy distribution for the free stream flow

4.3 Discussion of obtained distributions

The study of the recombination parameter of a TPS material in the VKI Plasmatron facility requires the use reference probes (two, according to the methodology followed) which, together with the sample material of interest, are subjected to the same plasma flow. Hence, the enthalpy of the flow is the same for all the probes. This represents the cornerstone of this study, where assumptions can be relaxed based on the fact that the enthalpy seen by all the probes are the same for the given conditions.

To compute the relationship between the boundary layer edge enthalpy and the catalytic parameter, the measurements obtained during the experiments are used as variables for the boundary layer code depicted before. This relationship presents a S-shape, since higher catalysis parameters lead to a lower enthalpy due to the higher effective atoms recombination implying lower energy content on the free stream. From these S-curves, the range of values possible for the enthalpy can be estimated: the minimum enthalpy corresponds to the maximum enthalpy possible for the material with lower catalytic properties and the maximum enthalpy corresponds to the minimum enthalpy of the material with higher catalytic properties.

As there are uncertainties associated with the measurements and model parameters, the S-curves also have uncertainty limits where the actual curve is contained within. These limits are computed considering the uncertainty of the heat fluxes and wall temperatures. The influence of the static and dynamic pressures uncertainties is not considered since these pressures play a minor role due to their small uncertainties. Moreover, they are common quantities to the three materials, thus, when they change, all curves move together, leaving the problem of the inference unchanged. Thereafter, the upper limit of the S-curve is computed with the maximum wall heat flux and wall temperature estimated considering their uncertainties and the lower limit computed with their minimum values.

The uncertainties from Table 2 correspond to a 2σ uncertainty level, meaning that are computed with a 95% confidence interval, being only the 5% of the samples outside of this range. When this interval is small for the solution to lay on, 3σ uncertainty limits are also computed, i.e., a 99% confidence interval.

To study the influence of pressure and heat flux on the TPS recombination parameter, reference heat fluxes for copper of 500, 700 and 900 kW/m² for static pressures of 15 and 100 mbar, and also 700 kW/m² for 50 mbar are analysed, relying on the values measured at the Plasmatron facility. The mean value for the recombination parameters of the TPS material and enthalpy, and extremes for a 95% confidence interval are summarized in Tables 3 and 4. These extremes are the results of the k th percentile: the lower piece of the distribution contains k % of the data and the upper piece contains (100- k)%. Hence, for a 95% confidence interval, the 2.5th and 97.5th percentiles leave, respectively, 2.5% of the data below and 2.5% beyond the respective point.

For the lowest pressure ($P_s = 15$ mbar) and higher reference heat fluxes (700 and 900 kW/m²), these cases depict a bimodal posterior distributions for the TPS material. In each case, both peaks match best the numerical equations, obeying the rebuilding condition $q_{meas} = q_{num}$. This phenomena is caused by the wide range of values possible for the enthalpy and can be caused by epistemic uncertainties. To improve the results under these testing conditions, a better prior distribution for copper and quartz can be used, based on knowledge from previous works.

Due to these bimodal distributions, the samples with higher probability fall into two different groups, decreasing the probability density among them. Consequently, they also present a wide standard deviation for TPS and enthalpy

Table 3: TPS material posterior distribution mean values and respective 2.5th and 97.5th percentiles.

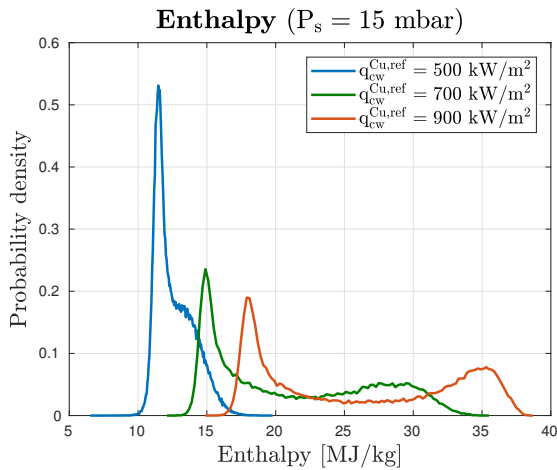
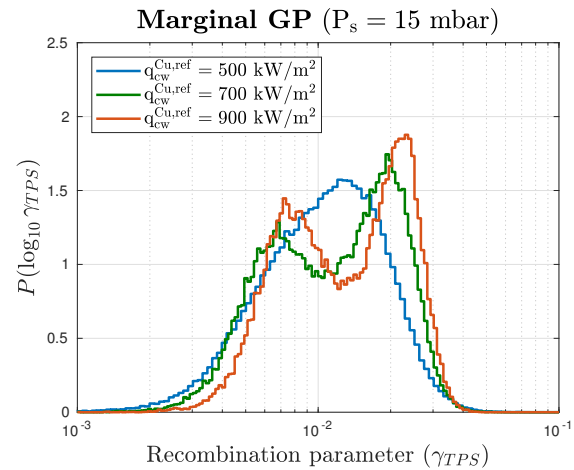
Test case	2.5th γ_{TPS}	Mean γ_{TPS}	97.5th γ_{TPS}
MTAt1	0.0029	0.0120	0.0276
MTAt2	0.0036	0.0134	0.0289
MTAt3	0.0044	0.0147	0.0303
MTAt4	0.0030	0.0049	0.0076
MTAt5	0.0035	0.0083	0.0167

Table 4: Enthalpy distribution mean values and respective 2.5th and 97.5th percentiles (in MJ/kg).

Test case	2.5th H_e	Mean H_e	97.5th H_e
MTAt1	10.8492	12.5977	15.6939
MTAt2	14.3012	21.0952	31.6738
MTAt3	17.3042	26.0089	36.6972
MTAt4	13.9420	14.6995	15.5160
MTAt5	10.7070	11.2314	11.7568

distributions. This phenomena can be analysed in Fig. 19, where the enthalpy for the three first test cases are represented. From this figure, as the range of possible enthalpy becomes wider (for higher heat fluxes), the maximum probability peak decreases and the second peak increases. Moreover, as expected, when the reference heat flux increases, also the mean enthalpy of the flow increases (as also concluded from Table 4).

Figure 20 illustrates the variation of the TPS distribution when the reference heat flux is increased, for the lowest static pressure tested ($P_s = 15$ mbar). Under this condition, all three distributions present a similar range of possible values for the recombination parameter and a very similar mean (see Table 3). Hence, one can conclude that for low pressures, the TPS catalytic parameter is not influenced by the enthalpy of the flow.

Figure 19: Variation of enthalpy distribution with reference heat flux, for $P_s = 15$ mbar.Figure 20: Variation of TPS distribution with reference heat flux, for $P_s = 15$ mbar.

For the last three experimental cases, the static pressure corresponds to 100 mbar. Under this condition, the separation between the S-curves is higher. In fact, even with a 99% confidence interval, only for the lowest heat flux ($q_{ref} = 500$ kW/m²) there is a range of enthalpy possible. For this case, the TPS posterior distribution presents a well-defined peak as the samples lay on a high gradient zone of the S-curve. As the posterior distribution is well-defined also the enthalpy distribution presents a well-defined peak, with low standard deviation.

Even though the first three test cases present a solution, for low pressure the LTE assumption for the boundary layer edge is questionable. At low pressure, there is a small amount of chemical reactions occurring, hence, the number of collisions may not be enough to reach equilibrium. Nevertheless, in each experimental test, the three probes are under the same flow being the error committed by this assumption similar in order of magnitude for all the results and, therefore, does not affect much the result for γ .

When comparing the evolution of the TPS distribution with the pressure for the same reference heat flux (Figs. 21 and 22), and even though enthalpies are different, as a first conclusion, one can see that the mean value for the recombination parameter decreases as the pressure increases. This increase of pressure causes more recombinations in the gas and influences the diffusion process, consequently diminishing the recombination at the wall and, thereafter, decreasing the mean value of the recombination parameter that explains the experimental data.

CHARACTERIZATION UNDER UNCERTAINTY OF CMC MATERIALS

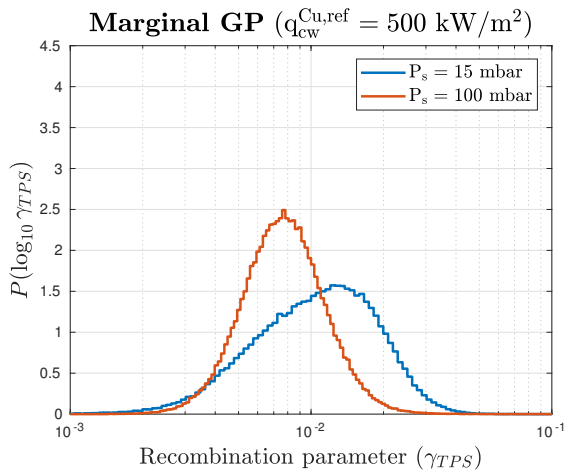


Figure 21: Variation of TPS distribution with static pressure for $q_{cw}^{Cu,ref} = 500 \text{ kW/m}^2$.

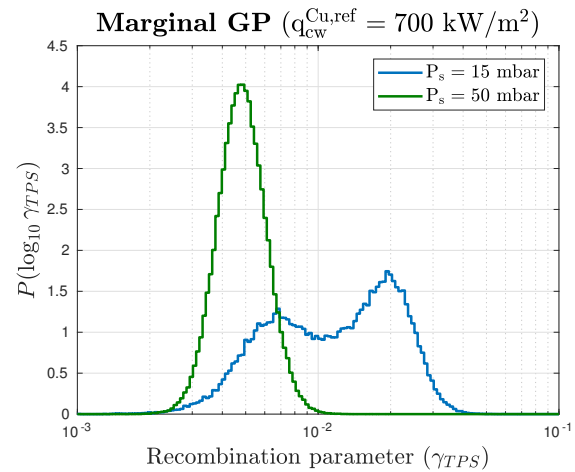


Figure 22: Variation of TPS distribution with static pressure for $q_{cw}^{Cu,ref} = 700 \text{ kW/m}^2$.

For the cases where there is no apparent solution for the enthalpies, the majority of the samples for the reference materials lay outside of the uncertainty limits, hence the solutions violate the variability of the measurements. For each of these cases, the distributions for q_{meas} and q_{num} , for both copper and quartz, do not match. Even though the TPS distributions match, i.e. $q_{meas} = q_{num}$, the reference materials do not have a successful inference, hence the overall inference cannot be trusted.

In the event of non-existence of a solution for the enthalpy, the likelihood algorithm tries to fit the measurements with the points with lowest error, even though further apart than what is expected from the uncertainties. Although the samples computed are the best fit for the numerical models, they are not good enough to match the heat flux distributions and the results are not physical. In these cases (at high static pressures), there is a plentiful of chemical reactions occurring in the boundary layer. In fact, Paneral⁵ compared different chemical models when constructing the S-curves and, for high pressures, the model chosen influences these curves considerably. Thereafter, the chemical models implemented in the numerical solvers are not good to capture the physics underlying the flow characteristics.

5. Concluding remarks

Experiments in the Plasmatron facility enable characterizing the catalytic properties of a TPS sample by combining direct measurements and a numerical reconstruction based on boundary layer simulations. However, experimental and numerical models are subjected to uncertainties, which must be taken into account during the inference process. The Bayesian inference approach followed in this work combines all set of available measurements to infer the catalytic properties of the ceramic materials considering measurement and model uncertainties.

In this work, a comprehensive study concerning the catalytic properties of thermal protection systems was carried, based on experiments performed at the VKI Plasmatron, under a proper Bayesian inference framework for uncertainties estimation.

This 3-probes testing methodology proved to be a good experimental approach to characterize ceramic materials of typical use in today's spacecraft. The fact that the TPS material laid in between the two materials at the opposite limits of its catalytic behaviour (copper and quartz), made the determination of the CMC material behavior more certain. Overall, the posterior distributions and enthalpy presented peaky and narrow distributions. For the cases whose S-curves were very close together, the range of possible enthalpies was very wide, making the TPS posterior distributions yield bimodal distributions, due to the similar support given by the similar behavior of each of the materials.

For low static pressures, when varying the reference heat flux and, consequently, the wall heat fluxes, temperatures, enthalpies and flow velocities, all the cases presented TPS posterior distributions with a very similar mean and interval range. Hence, one can conclude that, for the same low pressure, the TPS catalytic parameter is not influenced by the conditions of the flow. When increasing the static pressure, the distance between the S-curves increases, leading to non-existence of a solution, meaning that the catalytic properties cannot be inferred. In these cases, the chemical models implemented in the numerical solvers are not good to capture the underlying chemical reactions occurring in the boundary layer. For the same reference heat flux, when increasing the pressure, the catalytic parameter of the TPS material decreases, as expected. This increase of pressure leads to more recombination in the gas and, consequently, to less recombination at the wall.

Overall, the Bayesian inference framework proved to be a reliable way of characterizing ceramic materials

with proper uncertainty distributions. In this approach, no assumptions are made concerning the reference materials (copper and quartz), which are estimated together with the TPS material parameter with no differences in their prior knowledge. Additionally, no assumptions are made for the enthalpy of the flow, being the distribution of this parameter also estimated during the rebuilding process.

6. Acknowledgments

The research of A. del Val is fully funded by the European Commission H2020 programme, through the UTOPIAE Marie Curie Innovative Training Network, H2020-MSCA-ITN-2016, Grant Agreement number 722734. Prof. Thierry Magin is acknowledged for his help and guidance. Andrea Fagnani, Alan Viladegut, Bernd Helber and Pascal Collin are acknowledged for their help and advice during the experimental campaign and post-processing of the measurements.

References

- ¹ O. Chazot and F. Panerai. *High enthalpy facilities and plasma wind tunnels for aerothermodynamics ground testing in: Hypersonic Nonequilibrium Flows: Fundamentals and Recent Advances*. Ed. Eswar Josyula ARLF, 2015.
- ² T. Magin. *A Model for Inductive Plasma Wind Tunnels*. PhD thesis, ULB/VKI, 2004.
- ³ B. Laub and E. Venkatapathy. Thermal protection system technology and facility needs for demanding future planetary missions. In *Proceedings of international workshop on planetary probe atmospheric entry and descent trajectory analysis and science*, pages 239 – 247, 2004.
- ⁴ R. Goulard. On catalytic recombination rates in hypersonic stagnation heat transfer. *Journal of Jet Propulsion*, 28(11):737–745, November 1958.
- ⁵ F. Panerai. *Aerothermochemistry Characterization of Thermal Protection Systems*. PhD thesis, von Karman Institute for Fluid Dynamics and Università degli Studi di Perugia, 2012.
- ⁶ A. Viladegut. *Assessment of Gas-Surface Interaction Modelling for Lifting Body Re-Entry Flight Design*. PhD thesis, von Karman Institute for Fluid Dynamics and Universitat Politècnica de Catalunya, 2017.
- ⁷ F. Sanson, F. Panerai, T. E. Magin, and P. M. Congedo. Robust reconstruction of the catalytic properties of thermal protection materials from sparse high-enthalpy facility experimental data. *Experimental Thermal and Fluid Science*, 96:482–492, 2018.
- ⁸ B. Bottin, O. Chazot, M. Carbonaro, V. Van Der Haegen, and S. Paris. The VKI Plasmatron characteristics and performance. *Measurement Techniques for High Enthalpy and Plasma Flows*, April 2000.
- ⁹ B. Bottin. *Aerothermodynamic Model of an Inductively-Coupled Plasma Wind Tunnel: Numerical and Experimental Determination of the Facility Performance*. PhD thesis, von Karman Institute for Fluid Dynamics, 1999.
- ¹⁰ B. Helber. Calibration curves. Private communication.
- ¹¹ A. Lani, N. Villedieu, K. Bensassi, L. Kapa, M. Vymazal, M. S. Yalim, and M. Panesi. COOLFluid: an open computational platform for multi-physics simulation and research. In *21st AIAA Computational Fluid Dynamics Conference*, San Diego, CA, 2013.
- ¹² D. LeQuang. *Spectroscopic measurements of sub- and supersonic plasma flows for the investigation of atmospheric re-entry shock layer radiation*. PhD thesis, von Karman Institute for Fluid Dynamics and Université Blaise Pascal, 2014.
- ¹³ G. Degrez, P. Barbante, M. de la Llave, T. Magin, and O. Chazot. Determination of the catalytic properties of TPS materials in the VKI ICP facilities. In *European Congress on Computational Methods in Applied Sciences and Engineering - ECCOMAS Computational Fluid Dynamics Conference*, Swansea, Wales, UK, September 2001.
- ¹⁴ P. F. Barbante. *Accurate and efficient modelling of high temperature nonequilibrium air flow*. PhD thesis, von Karman Institute for Fluid Dynamics and Université Libre de Bruxelles, 2001.
- ¹⁵ F. Sanson, N. Villedieu, F. Panerai, O. Chazot, P. M. Congedo, and T. E. Magin. Quantification of uncertainty on the catalytic property of reusable thermal protection materials from high enthalpy experiments. *Experimental Thermal and Fluid Science*, 82:414–423, 2017.

CHARACTERIZATION UNDER UNCERTAINTY OF CMC MATERIALS

- ¹⁶ D. S. Sivia and J. Skilling. *Data Analysis: A Bayesian tutorial*. Oxford Science Publications, 2006.
- ¹⁷ J. A. Nelder and R. Mead. A simplex method for function minimization. *Computer Journal*, 7(4), January 1965.
- ¹⁸ M. D. McKay, R. J. Beckman, and W. J. Conover. A comparison of three methods for selecting values of input variables in the analysis of output from a computer code. *Technometrics*, 21(2):239–245, May 1979.
- ¹⁹ C. E. Rasmussen and C. K. I. Williams. *Gaussian Processes for Machine Learning*. the MIT Press, 2006.
- ²⁰ J. Kaipio and E. Somersalo. *Statistical and Computational Inverse Problems*. Springer-Verlag, 2005.
- ²¹ A. Fagnani. Plasma testing methodology for demise phenomena analysis. Project report, von Karman Institute for Fluid Dynamics, June 2018.
- ²² B. Helber. *Material Response Characterization of Low-density Ablators in Atmospheric Entry Plasmas*. PhD thesis, von Karman Institute for Fluid Dynamics and Vrije Universiteit Brussel, January 2016.